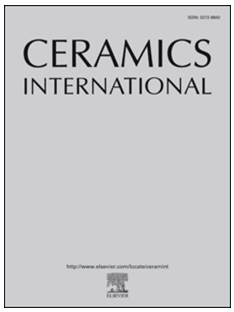

Molten salt synthesis of Ce doped zirconolite for the immobilisation of pyroprocessing wastes and separated plutonium

Amber R. Mason, Florent Y. Tocino, Martin C. Stennett, Neil C. Hyatt

PII: S0272-8842(20)32458-5

DOI: https://doi.org/10.1016/j.ceramint.2020.08.080

Reference: CERI 26182

To appear in: *Ceramics International*

Received Date: 7 May 2020

Revised Date: 30 July 2020

Accepted Date: 10 August 2020

Please cite this article as: A.R. Mason, F.Y. Tocino, M.C. Stennett, N.C. Hyatt, Molten salt synthesis of Ce doped zirconolite for the immobilisation of pyroprocessing wastes and separated plutonium, *Ceramics International* (2020), doi: https://doi.org/10.1016/j.ceramint.2020.08.080.

Molten salt synthesis of Ce doped zirconolite for the immobilisation of pyroprocessing wastes and separated plutonium

Amber R. Mason, Florent Y. Tocino, Martin C. Stennett, Neil C. Hyatt*

Immobilisation Science Laboratory, Department of Materials Science and Engineering, University of Sheffield, Sir Robert Hadfield Building, Sheffield S1 3JD, UK

**To whom correspondence should be addressed. Email n.c.hyatt@sheffield.ac.uk, phone +44 (0) 114 222 5470, fax +44 (0) 114 222 5943*

ABSTRACT

Molten salt mediated synthesis of zirconolite $Ca_{0.9}Zr_{0.9}Ce_{0.2}Ti_2O_7$ was investigated, as a target ceramic matrix for the clean-up of waste molten salts from pyroprocessing of spent nuclear fuels and the immobilisation of separated plutonium. A systematic study of reaction variables, including, reaction temperature, time, atmosphere, reagents and composition, was made to optimise the yield of the target zirconolite phase. Zirconolite 2M and 3T polytypes were formed as the major phase (with minor perovskite) between 1000 – 1400 °C, in air, with the relative proportion of 2M polytype increasing with temperature. Synthesis under 5% H_2/N_2 or Ar increased the proportion of minor perovskite phase and reduced the yield of the zirconolite phase. The yield

of zirconolite polytypes was maximised with the addition of 10 wt.% TiO_2 and 5 wt.% TiO_2, yielding 91.7 ± 2.0 wt.% zirconolite, primarily as the 2M polytype, after reaction at 1200 °C for 2 h, in air. The particle size and morphology of the zirconolite product bears a close resemblance to that of the TiO_2 precursor, demonstrating a dominant template growth mechanism. Although the molten salt mediated synthesis of zirconolite is effective at lower reaction temperature and time, compared to reactive sintering, this investigation has demonstrated that the approach does not offer any clear advantage with over conventional reactive sintering for the envisaged application.

Keywords: nuclear applications (E), spectroscopy (B), molten salt synthesis

1. INTRODUCTION

Pyrochemical reprocessing (pyroprocessing) is an advanced method of recycling spent nuclear fuel (SNF) where the U, Pu and minor actinides (MA) are separated from the fission products (FP) by electrorefining in a molten salt eutectic [1]. An advantage of pyroprocessing over conventional aqueous reprocessing is that a separated Pu stream is no longer generated, which reduces the associated proliferation risk [2]. The waste stream generated via this process is typically a chloride salt eutectic with entrained MA and FP, plus trace residual Pu. Chloride rich waste streams such as these are challenging to immobilise using traditional high level waste (HLW) immobilisation methods since the chloride anion has low solubility in borosilicate glasses, which have, hitherto, been applied for HLW immobilisation [3]–[7].

Zirconolite (prototypically $CaZr_xTi_{3-x}O_7$ where $0.8<x<1.35$) is a crystalline titanate ceramic material and is the targeted actinide host phase in SYNROC C [8]. It exists in the space group C2/c and has several polytypes: 2M, 3O, 3T, 4M and 6T, with the most common being the monoclinic 2M structure [8–11]. In the 2M structure, Ca and Zr adopt 8- and 7-fold coordination, respectively, as CaO_8 and ZrO_7 polyhedra; whereas, Ti adopts mixed 6-fold and 5-fold coordination, as TiO_6 and TiO_5 polyhedra, with the latter site being 50% occupied [12]. Synthetic zirconolite has natural analogue minerals retaining lanthanides and actinides dated to be millions or hundreds of millions of years old, which further demonstrates its long-term radiation stability and chemical durability over geological timescales [13–16]. The lanthanide and actinide elements are usually found on the Ca site with charge balancing cations, such as Al or Mg, on the Ti site [8,16].

Molten salt synthesis (MSS) is a method of producing ceramic materials which typically uses a chloride salt eutectic to reduce the diffusion distance of the ceramic reagents. This method generally produces a material that is homogeneous at a lower synthesis temperature and reaction time compared to traditional solid state synthesis methods [17]. The chloride salts can be dissolved upon completion of the reaction to recover the synthesised ceramic material. Conventional solid state synthesis of zirconolite, requires reactive sintering at 1450 °C for several hours, often with several cycles of heat treatment and intermittent grinding [18]. In comparison, zirconolite can be synthesised at 1200 °C in only a few hours, in the presence of a NaCl:KCl molten salt eutectic, with a melting point of approximately 658 °C [19]. There are two bounding mechanisms observed in the MSS of ceramic materials: dissolution-precipitation and template growth [20–25], which are dependent on the solubility of ceramic reagents in the salt eutectic. Dissolution-precipitation is favoured when all reagents are comparably soluble in the salt eutectic and subsequently react to form a product. Template growth occurs when one reagent is less soluble and acts as a template onto which the other more soluble reagents are deposited, at which point the product is formed. This mechanism allows the microstructure of the sample to be controlled resulting in uniform grain size and morphology.

This investigation seeks to develop the approach of decontaminating the chloride molten salt waste from pyroprocessing, by using the salt itself as a medium for the synthesis of a titanate ceramic wasteform to incorporate the long lived lanthanides, MA and trace Pu [4,26–29]. Zirconolite was selected as

the titanate ceramic wasteform, with Ce utilised as a non-active structural surrogate for the actinide and lanthanide elements due to having a similar ionic radius, accessible oxidation states, and crystal chemistry [30–32]. The target composition for the wasteform was $Ca_{0.9}Zr_{0.9}Ce_{0.2}Ti_2O_7$, where Ce was substituted on both the Ca and Zr sites. This is a charge compensated composition, targeting an equal proportion of Ce^{3+} ions on the Ca and Zr sites, without the requirement of additional charge compensating species on the Ti site. The target formulation was devised to incorporate Ce, as a MA / Pu surrogate, at a realistic concentration for a conceptual ceramic wasteform.

The NaCl:KCl eutectic composition was chosen as a model system relevant to wastes arising from pyrochemical reprocessing of mixed oxide $(U,Pu)O_2$ fuels using the Dimitrovgrad Dry Process at the Research Institute for Atomic Reactors in Russia and early pyrochemical reprocessing of short cooled Experimental Reactor Breeder II metallic fuel at Argonne National Laboratory – West (now Idaho National Laboratory), USA [33,34]. Additionally, a NaCl:KCl eutectic was used in experimental pyrochemical reprocessing of thorium high temperature reactor fuels undertaken at Joint Research Centre-Institute for Trans Uranium Elements (JRC-ITU) [35]. The UK is also undertaking strategic assessment of pyrochemical recycle of used nuclear fuels, including design and demonstration of wasteforms for decontamination and immobilisation of lanthanides and residual actinides from alkali chloride molten salts.

A further motivation for our research is management of the UK plutonium stockpile, which is projected to exceed 140 tons at the end of current reprocessing options [27]. A significant fraction of the plutonium stockpile will

require immobilisation in a suitable waste form, since it is unsuitable for reuse in MOX fuel, which is the preferred management approach at the present time [34]. Some of this material is contaminated by chlorine, as a result of the degradation of the polyvinylchloride packaging used to store the material [28]. A zirconolite ceramic is the leading candidate waste form for immobilisation of this stockpile and, therefore, a rapid and low temperature MSS process could be advantageous for ceramic waste form manufacture, given the presence of chlorine as a contaminant. Gilbert previously established the NaCl:KCl eutectic to be the most advantageous for zirconolite synthesis [19], although the yield was only 86 wt.% after reaction at 1000 °C. In contrast, the yield of zirconolite was 24 wt.% in the case of $CaCl_2$:NaCl eutectic at 1000 °C, whereas zirconolite failed to form when utilising a $MgCl_2$:NaCl eutectic. Note that this work focused the synthesis of the stoichiometric parent phase but did not consider the incorporation of a MA/Pu surrogate. Our choice of NaCl:KCl eutectic composition as the MSS medium was also made with due regard to potential application to the immobilisation of chloride contaminated plutonium stockpile material in a zirconolite ceramic, using Ce as a Pu surrogate.

2. MATERIALS AND METHODS

A NaCl:KCl eutectic (1:1 molar ratio) with a salt to ceramic molar ratio of 7:1 was primarily used in this study with the aim of producing single phase Ce doped zirconolite. To optimise the yield of the target zirconolite phase, the following reaction variables were systematically investigated: salt to ceramic ratio (3:1 – 9:1), synthesis temperature (1100 °C – 1400 °C), time at synthesis temperature (2 – 8 h), atmosphere (air, Ar or 5% H_2/N_2), Ce source (CeO_2 or $CeCl_3.7H_2O$), stoichiometric or excess quantities of ZrO_2 and TiO_2 reagents (excess, respectively, of 10 wt.% and 5 wt.%).

2.1. Materials

CaO (Alfa Aesar purity 98%), TiO_2 (anatase) (Sigma Aldrich, 99% purity), ZrO_2 (Sigma Aldrich, purity 99%), $CeCl_3.7H_2O$ (Sigma Aldrich, >99% purity) and CeO_2 (Fisher Scientific purity >99%) were used as reagents. NaCl (Sigma Aldrich, purity 99%) and KCl (Sigma Aldrich, purity 99%) were used as the molten salt flux. All reagents, with the exception of CaO and $CeCl_3.7H_2O$, were dried overnight at 180 °C before use.

2.2. MSS - $Ca_{0.9}Zr_{0.9}Ce_{0.2}Ti_2O_7$

A 1:1 molar ratio of NaCl and KCl was mixed (30 Hz, 5 mins) in a Fritsch Pulverisette 6 planetary mill with cyclohexane as a carrier fluid to produce the salt flux. Stoichiometric quantities of ceramic reagents were weighed according to the composition $Ca_{0.9}Zr_{0.9}Ce_{0.2}Ti_2O_7$ and mixed using the same conditions as the salt flux. A short mixing time was used to prevent size reduction of the reagents and preserve the particle morphology, to assist later assessment of

the role of templating or dissolution-precipitation reaction mechanism. A 0.5 g batch with a molar ratio of 7:1 salt eutectic:ceramic was mixed in a Fritsch Mini Mill 23 with cyclohexane as a carrier fluid (30 Hz, 5 mins). The resulting slurry was dried at ~95 °C, sieved through a 212 µm mesh to separate from the milling media. The powder was uniaxially pressed in a 10 mm hardened stainless-steel die with a 1 ton load and held for one minute to produce a green pellet. The green pellets were placed in an alumina crucible and heated in a muffle furnace to 300 °C for 1 h to remove any entrained moisture and then reacted at 1200 °C for 2 h in air with a 5 °C/min heating/cooling rate. The resulting reacted pellet was crushed into a fine powder using a pestle and mortar. The powder was washed with deionised water to remove the salt flux and vacuum filtration used to recover the product.

The above method was repeated with independent changes of experimental variables as follows: salt to ceramic ratio (3:1, 5:1 and 9:1), synthesis temperature (1100 °C, 1300 °C and 1400 °C), furnace atmosphere (flowing 5% H_2/N_2 and Ar), furnace dwell duration (4 h and 8 h) and varying excess of ZrO_2 and TiO_2 reagents. Additionally, materials were produced using $CeCl_3.7H_2O$ (Sigma Aldrich, >99% purity), as the MA / Pu surrogate, replacing CeO_2 in the ceramic batch.

After refinement of the experimental parameters discussed above, the optimum synthesis conditions were used to produce Ce doped zirconolite using MSS, with the resulting powder being uniaxially pressed into a ceramic body. The ceramic body was placed into a furnace and reacted in air at 1350 °C for 20 h, and the resulting ceramic was characterised.

2.3. Materials characterisation

Powder X-ray diffraction of reagents and products was performed with a Bruker D2 Phaser X-ray Diffractometer with a Ni filtered Cu Kα radiation (λ = 1.5418 Å) source, operating at 30 kV and 10 mA. Diffraction patterns were collected from $10° < 2\theta < 70°$ with a step size of 0.02° 2θ and dwell time of 38 s per step. The ICDD PDF-4+ database and ICSD sources were used to identify the phases present in each sample. The PDF numbers used for the pattern identification are: $CaZrTi_2O_7$ 2M (01-084-0163), $CaZrTi_2O_7$ 3T (01-072-7510), ZrO_2 (01-072-1669), TiO_2 (16-934), CeO_2 (01-081-0792) and $CaTiO_3$ (01-082-0228). XRD patterns were refined to provide quantitative phase analysis using the Bruker TOPAS software [36].

Secondary electron imaging of the microstructure of reagents and ceramic products was performed using a Philips XL 30 scanning electron microscope (SEM) at a working voltage of 20 kV. The powders were mixed with isopropanol in a beaker and placed in an ultrasonic bath. The resulting mixture was mounted onto aluminium pin stubs using carbon tabs, allowing for the isopropanol to evaporate before carbon coating.

The microstructure of the final sintered ceramic body was observed using a Hitachi TM3030 SEM with Oxford Instruments Swift ED3000 silicon drift detector. Energy dispersive X-ray spectroscopy (EDX) mapping was processed using the Bruker Quantax 70 software with maps collected for a minimum of 10

minutes. The ceramic body was mounted in epoxy resin, polished to a 1 µm optical finish and carbon coated prior to analysis.

The Ce oxidation state in each sample was determined from analysis of X-ray absorption spectroscopy data at the Ce L_3 edge (5723.0 eV). Measurements were conducted at the National Synchrotron Light Source II (NSLS-II) at Brookhaven National Laboratory (Upton, New York) on beamline 6-BM. NSLS-II operates at 3 GeV storage ring with a 400 mA current and 6-BM utilises a 3-pole wiggler to deliver X-rays in the energy range between 4.5 and 23 keV. The optical arrangement consists of a parabolic collimating mirror, a Si(111) monochromator, a toroidal focussing mirror, and a harmonic rejection mirror. For this study an unfocussed beam was used, and the beam size was limited to 0.5 mm in the vertical and 6 mm in the horizontal using slits. An ionisation chamber was used to measure the incident X-ray energy and the fluorescence signal was collected using a SII Vortex ME4 (4-element) Si drift detector. To optimise collection efficiency, the samples were mounted at 45° to both the incident X-ray beam and the vortex detector. The fluorescence signal was dead-time corrected as previously described in Woicik et al. [37]. Spectra were recorded between 5533 and 5965 eV with energy steps of 10 eV (5533 – 5693), 2 eV (5693 – 5713), 0.3 eV (5713 – 5783) and 0.05k (5783 – 5965). An accumulation time of 0.5 s $step^{-1}$ was used for the first three regions and 0.25k $step^{-1}$ for the final region. Multiple scans were collected for each sample and averaged to improve the signal to noise ratio. To ensure energy reproducibility (± 0.05 eV) a CeO_2 standard was measured simultaneously with each sample; the CeO_2 standard was placed downstream of the sample and the transmitted

intensity was measured using an ionisation chamber. Absolute energy calibration was performed by measuring a Cr foil and setting the position of the first inflection point in the derivative spectrum to 5989 eV [38]. Samples, and reference compounds, were prepared by homogenising finely powdered sample with polyethylene glycol and uniaxial pressing to form a 13 mm pellet with a thickness equivalent to 1 absorption length. Data reduction and linear combination fitting (LCF) were performed using the Athena software package [39] allowing the proportion of Ce^{3+} in each sample to be calculated.

3. RESULTS

We first attempted MSS of $Ca_{0.9}Zr_{0.9}Ce_{0.2}Ti_2O_7$ at 1200 °C with a 2 h reaction time, in air, and a salt to ceramic ratio of 7:1 on a molar basis (the synthesis conditions used by Gilbert to produce the parent $CaZrTi_2O_7$ zirconolite by MSS [19]). However, secondary phases of ZrO_2 and $CaTiO_3$ were observed (Figure 1). Based on these results, several experimental parameters were varied to achieve a single phase ceramic product (e.g. salt to ceramic ratio, temperature, dwell duration, atmosphere, Ce source, excess reagents). It is desirable that a single phase wasteform is obtained since the accessory perovskite phase may also act as a host for Ce/Pu but has comparatively poor aqueous durability and radiation tolerance [37]. We first investigated the effect of salt to ceramic ratio (3:1, 5:1, 7:1, 9:1) on the MSS of $Ca_{0.9}Zr_{0.9}Ce_{0.2}Ti_2O_7$ at 1200 °C, with a 2 h reaction time, in air. As shown in Figure S1, the phase assemblage was observed to be invariant comprising a major zirconolite 2M phase, minor perovskite, and trace zirconolite 3T, residual ZrO_2 and TiO_2 reagents. Accordingly, the salt to ceramic ratio was fixed at 7:1, on a molar basis, in the middle of the range investigated for further optimisation studies.

3.1 Characterisation of phase assemblage by X-ray diffraction

Figure 1 shows powder XRD patterns of the product recovered from MSS of nominal $Ca_{0.9}Zr_{0.9}Ce_{0.2}Ti_2O_7$ over the range 1100 to 1400 °C, with a reaction time of 2 h in air. All XRD patterns show the formation of zirconolite 2M and 3T polytypes, at all temperatures, together with evidence of residual ZrO_2 and TiO_2 reagents, and an accessory perovskite phase (prototypically $CaTiO_3$).

Quantitative phase analysis of the phase assemblage was undertaken, by Rietveld analysis of XRD data; the results are summarised in Table 1 and compared in Figure 2 (an example fit is shown in Figure S2). The quantitative phase analysis showed the overall yield of the zirconolite 2M phase to increase with reaction temperature, from 43.9 wt.% at 1100 °C, to 62.1 wt.% at 1400 °C (± 1.8 wt.%). A concomitant reduction in the fractions of residual ZrO_2 and TiO_2 reagents, accessory perovskite, and zirconolite 3T phase, were observed, with increasing reaction temperature. The combined fraction of zirconolite 2M and 3T phases increased from 54.9 wt.% at 1100 °C, to 74.3 wt.% (± 2.0 wt.%) at 1400 °C. The reaction temperature was not increased further since single phase Ce-doped zirconolites can be produced by conventional solid state synthesis at 1400 °C [19,20], and the MSS method of interest here would offer no meaningful advantage.

Overall, these data show that at 1100 °C, the yield of zirconolite 2M was hindered by slow reaction kinetics, at 1200 °C and higher temperature the yield of zirconolite 2M was increased by reaction of reagents and conversion of the zirconolite 3T to 2M polymorph. The overall yield of zirconolite phases increased by a greater margin when the reaction temperature was increased from 1100 °C to 1200 °C, compared to 1400 °C, which may reflect increased volatilisation of the molten salt medium. For subsequent optimisation, a reaction temperature of 1200 °C was selected, given the evidence for reasonable reaction kinetics balanced against minimising the reaction temperature to reduce evaporation of the molten salt and, with a view to process implementation, potential volatile fission products.

Following investigation of the phase assemblage produced by MSS as a function of reaction temperature, the effect of oxygen partial pressure was studied by imposing an atmosphere of 5% H_2/N_2 or Ar gas. Figure 3 compares the powder XRD patterns of the product recovered from MSS of nominal $Ca_{0.9}Zr_{0.9}Ce_{0.2}Ti_2O_7$ at 1200 °C, with a reaction time of 2 h in air, 5% H_2/N_2 and Ar. These data and the quantitative phase analysis summarised in Table 1 and Figure 2, show the reducing atmosphere to result in a markedly lower yield of zirconolite 2M and 3T phases. The combined yield of zirconolite 2M and 3T was 46.6 wt.% and 34.8 wt.% for the 5% H_2/N_2 and Ar atmosphere respectively, compared to 66.9 wt.% for air atmosphere (± 2.0 wt.%). Evident from the quantitative phase analysis is a greater fraction of residual ZrO_2 (15.6 – 17.3 ± 0.4 wt.%), which suggests that the solubility of ZrO_2 in the molten salt medium is strongly dependent on effective oxygen partial pressure, resulting in a lower yield of zirconolite and increased yield of perovskite (33.3 - 40.9 ± 1.0 wt.%). Ce L_3 XANES data demonstrated Ce to be completely reduced to Ce^{3+}, which is expected to stabilise the perovskite accessory phase as discussed further in Section 3.3, possibly assisted by the reduction of Ti^{4+} to Ti^{3+} within the sample. Begg and Clarke reported that annealing $CaZrTi_2O_7$ under 3.5 % H_2/N_2 atmosphere results in reduction of Ti^{4+} to Ti^{3+} [21,22], and the formation of a Zr rich zirconolite and perovskite. Our observations are consistent with this mechanism. Given the evident lower stability of the zirconolite phase under reducing conditions, further optimisation of the MSS reaction conditions applied a temperature of 1200 °C and air atmosphere.

Figure 4 compares the powder XRD patterns of the product recovered from MSS of nominal $Ca_{0.9}Zr_{0.9}Ce_{0.2}Ti_2O_7$ after reaction at 1200 °C, with a reaction time of 2 h, 4 h or 8 h in air. These data show a broadly similar phase assemblage, with quantitative phase analysis, summarised in Table 1 and Figure 2, revealing relatively small changes in phase fraction, close to the estimated margin of precision. In particular, the total yield of zirconolite phases did not show a marked increase with reaction time, with changes being close to the estimated precision of ± 2.0 wt.%. This observation is consistent with evaporation of the molten salt medium with increased reaction time, and with diffusion – reaction occurring primarily in the solid state, for which the reaction kinetics to yield zirconolite are known to be low at 1200 °C [19,20]. The quantitative phase analysis of the product from reaction at 1200 °C in air for 4 h showed an anomalously high fraction of residual ZrO_2 reagent, 3.9 ± 0.4 wt.%, the origin of which is unclear, but is consistent with a marginally lower yield of the target zirconolite phase. For the purpose of further optimisation of the MSS process, therefore, the reaction conditions were fixed at 1200 °C, for a duration of 2 h, under air.

With processing conditions of 1200 °C for 2 h in air, optimised from the investigations above, the addition of excess ZrO_2 and TiO_2 reagents was explored, with the aim of consuming the perovskite accessory phase. Figure 5 shows the powder XRD data pattern of the product recovered from MSS of nominal $Ca_{0.9}Zr_{0.9}Ce_{0.2}Ti_2O_7$ after reaction at 1200 °C, for 2 h, in air, with an excess of 10 wt.% ZrO_2 and 5 wt.% TiO_2 reagents. Quantitative phase analysis, Table 1 and Figure 2, showed that this adjustment of the reaction composition

was successful and reduced the fraction of perovskite accessory phase to 9.4 ± 1.0 wt.%, with the yield of zirconolite 2M increased to 64.3 ± 0.8 wt.%. The overall yield of zirconolite 2M and 3T phases, combined, increased to 83.6 ± 2.0 wt.%, with ca. 5 wt.% of unreacted reagents.

The use of $CeCl_3$ as a reagent and actinide surrogate, was also explored since MA and Pu will be incorporated as a chloride species with the molten salt in a pyroprocessing waste stream, unless precipitated as an oxide by oxygen sparging [41]. Figure 5 presents the powder XRD data pattern of the product recovered from MSS of nominal $Ca_{0.9}Zr_{0.9}Ce_{0.2}Ti_2O_7$ after reaction at 1200 °C, for 2 h, in air, using $CeCl_3.7H_2O$ as the Ce source, with and without an excess of 10 wt.% ZrO_2 and 5wt.% TiO_2 reagents. The overall yield of zirconolite 2M and 3T phases, combined, was, respectively, 68.9 wt.% and 62.8 wt.% (± 2.0 wt.%) for the formulations with and without an excess of 10 wt.% ZrO_2 and 5 wt. % TiO_2. The use of $CeCl_3.7H_2O$ evidently has a detrimental effect on the phase assemblage, compared to the use of CeO_2, with a reduced yield of zirconolite. This is correlated with the residual ZrO_2 phase fraction being approximately three times greater in the products of reaction utilising $CeCl_3.7H_2O$ compared to CeO_2, suggesting the lower yield may arise from lower ZrO_2 solubility.

The final step in this study involved sintering of the product of $Ca_{0.9}Zr_{0.9}Ce_{0.2}Ti_2O_7$ MSS, produced at 1200 °C, for 2 h, in air with an excess of 10 wt.% ZrO_2 and 5 wt.% TiO_2, using CeO_2 as a Ce source. The sintering conditions were 1350 °C for 20 h in air, and X-ray diffraction, Figure 6, coupled with quantitative phase analysis, demonstrated the combined zirconolite 2M, 4M and 3T polymorphs to comprise 91.7 ± 2.0 wt.% of the phase assemblage, with

345 the 2M polymorph (75.9 ± 1.8 wt.%) as the major component. A minor
346 perovskite accessory phase was determined (7.3 ± 1.0 wt.%) with the trace
347 CeO_2, ZrO_2 and TiO_2 (combined 1.0 ± 0.5 wt.%).

348

349 ***3.2. SEM/EDX characterisation***

350 The scanning electron micrographs in Figure 7 show the morphology of each
351 reagent, along with that of the $Ca_{0.9}Zr_{0.9}Ce_{0.2}Ti_2O_7$ product of MSS at 1200 °C
352 for 2 h, in air (with CeO_2). Comparison of the particle morphology of the
353 reagents and the product material, shows that the primary particle size and
354 habit of the product is similar to that of the TiO_2 reagent (~ 1 µm) and clearly
355 differentiated from the that of the CeO_2 and ZrO_2 reagents, with much larger
356 and smaller particle size, respectively. This suggests that template growth is the
357 mechanism by which $Ca_{0.9}Zr_{0.9}Ce_{0.2}Ti_2O_7$ was produced. The faceted nature of
358 TiO_2 reagent (see Figure 7 (a)) was reflected in the habit of the
359 $Ca_{0.9}Zr_{0.9}Ce_{0.2}Ti_2O_7$ product (Figure 7 (d)). However, it was evident that some
360 growth in product particle size had occurred, relative to the TiO_2 reagent, which
361 provides evidence for a contribution of dissolution – precipitation and/or solid
362 state diffusion, to the overall synthesis mechanism.

363 The microstructure of the sintered $Ca_{0.9}Zr_{0.9}Ce_{0.2}Ti_2O_7$ ceramic is shown in
364 Figure 8. The material comprises a majority matrix (mid grey) of the zirconolite
365 2M polymorph, with inclusions of ZrO_2 (bright grey) and small isolated
366 perovskite grains (dark grey). The zirconolite 3T polymorph cannot be
367 differentiated from the 2M polymorph, presumably due to similar composition

and hence back scattered electron contrast, combined with its low abundance. The average EDX determined composition of the combined zirconolite 2M and 3T phases, was $Ca_{0.95(3)}Zr_{0.88(3)}Ce_{0.17(2)}Ti_{2.01(2)}O_7$, in reasonable agreement with the target stoichiometry. This implies an average Ce oxidation state of $Ce^{3.2+}$, within the zirconolite phase.

The zirconolite 4M phase is apparent as a small variation to the matrix contrast, which arises from a slightly higher Ce concentration as judged from EDX data. The microstructure is relatively well sintered although isolated porosity is apparent.

3.3. Ce L_3 XANES

Ce L_3 XANES data were acquired from product materials as a probe of the average Ce oxidation state and are shown in Figure 9. The spectra were analysed using linear combination fitting (LCF) to estimate the proportion of Ce^{3+} in each product, using reference spectra of CeO_2 (for 8-fold coordinated Ce^{4+}), $CeAlO_3$ (for 12-fold coordinated Ce^{3+}) and $CePO_4$ (monazite; for 9-fold coordinated Ce^{3+}). Spectra were fitted over the range 5700 – 5760 eV, under the constraint that the fractional weights of the reference spectra sum to unity; the results are summarised in Table 2 with an example fit shown in Figure S3. Note that the Ce L_3 XANES of $CePO_4$ and $CeAlO_3$ present a single intense feature on the rising absorption edge, whereas CeO_2 presents three features, of lower relative intensity, for which the corresponding final state electron configurations were previously assigned [42–45].

The Ce L_3 XANES data and LCF analysis (Figure 9A; Table 2), showed the fraction of Ce^{3+} to increase with increasing reaction temperature (with constant reaction time of 2h, in air), which is expected for the autoreduction of CeO_2 [46]; this was correlated with the concomitant increase in the combined fraction of major zirconolite 2M and 3T polytypes, and reduction in the perovskite fraction, in the phase assemblage (Table 1). In contrast, the fraction of Ce^{3+} increased only marginally when the reaction time was extended from 2h to 8h (Figure 9C; Table 2), consistent with only a small increase in the combined fraction of major zirconolite 2M and 3T polytypes, and reduction in perovskite phase fraction (Table 1). Taken together, these data show that the total yield of zirconolite and Ce^{3+} fraction increase with increasing temperature, according to the target

formulation, by reaction of the perovskite accessory phase and residual TiO_2 and ZrO_2. It is evident, however, that the zirconolite product must incorporate some proportion of Ce^{4+}.

Synthesis in a reducing atmosphere showed a complete reduction of Ce with the fraction of Ce^{3+} being 100 ± 4% for both 5% H_2/N_2 and Ar products (Figure 9B). This was accompanied by a significant decrease in zirconolite yield in contrast with the effect of increasing temperature on phase assemblage. This implies that when the Ce^{3+} content increases above ca. 60%, the competing perovskite phase is stabilised, which provides a 12 co-ordinate site to accommodate the larger Ce^{3+} species [49]. The proportion of perovskite phase is similar to the ~ 40 wt.% observed in the phase assemblage produced from conventional reaction sintering of $CaZr_{0.6}Ce_{0.2}Ti_2O_7$ ceramics under H_2/N_2 and Ar, with a Ce^{3+} content of 80 – 100% [47].

Substituting $CeCl_3$ for CeO_2 as the Ce source, resulted in reduction of the Ce^{3+} fraction from 59 ± 3% to 38 ± 3%, in the products from reaction at 1200 °C for 2 h, in air; however, this was not accompanied by a significant change in the overall phase assemblage. The effect of addition of 10 wt.% ZrO_2 and 5 wt.% TiO_2 to the formulation resulted in marked reduction of the Ce^{3+} fraction from 59 ± 3% to 33 ± 3%, in the product from reaction at 1200 °C for 2h, in air, correlated with the maximum yield in of combined zirconolite 2M and 3T polytypes in the phase assemblage (Table 1); this is also the case when CeO_2 is replaced by $CeCl_3$, although to less extent. Taken together, these data demonstrate a strong effect of the addition of excess 10 wt.% ZrO_2 and 5 wt.%

425 TiO_2 in increasing the total yield of the zirconolite product, which must
426 incorporate a higher fraction of Ce^{4+}.

427 Figure 10 shows a comparison between the average Ce oxidation state (from
428 Table 2) and the weight fraction of perovskite formed in each product. There is a
429 general trend of increasing perovskite content associated with a greater the
430 quantity of Ce^{3+} in the sample at a constant synthesis temperature. As noted
431 above, the competing perovskite phase provides a 12 co-ordinate site to
432 accommodate the larger Ce^{3+} species [40], and hence the proportion of the
433 perovskite phase increases with increasing Ce^{3+} content, which is generally
434 associated with a lower yield of zirconolite.

435

436 **4. DISCUSSION**

437 Ce doped zirconolite was synthesised in a NaCl:KCl molten salt eutectic, as a
438 conceptual process for decontamination of pyroprocessing molten salt wastes
439 and immobilisation of separated plutonium. The presence of a molten salt
440 eutectic enables synthesis of zirconolite at 1200 °C in 2 h, in air, considerably
441 reduced compared to conventional reaction sintering which requires e.g. 1400
442 °C for 20 h. Interestingly, our investigation yields zirconolite 2M, 3T and 4M
443 polytypes, with evidence for conversion of 3T to 2M, with increasing
444 temperature. In contrast, similar compositions fabricated by conventional
445 reactive sintering comprise only the 2M polytype, with minor 4M polytype when
446 synthesised under air [48]. Our data are consistent with previous studies of
447 NaCl:KCl and $CaCl_2$:NaCl molten salt synthesis of the parent $CaZrTi_2O_7$
448 zirconolite, which identified the formation of the 3T polytype, as the major phase

after reaction at 1100 °C, giving way to formation of the 2M polytype at 1200 °C [19]. The zirconolite 3T phase therefore appears to be a low temperature metastable polytype structure.

Molten salt mediated synthesis yields products with a minimum Ce^{3+} content at least 33% greater than similar compositions synthesised by reactive sintering in air, when using CeO_2 as a reagent. Therefore, the mechanism of Ce solubility in the NaCl-KCl eutectic appears to involve reduction of Ce^{4+} to Ce^{3+}, yielding products with relatively high Ce^{3+} content. We are not aware of solubility data for Ce^{4+} / Ce^{3+} in chloride molten salts, but this conclusion is consistent with chloride molten salt mediated synthesis of CeOCl from CeO_2 [48]. Interestingly, the analogous $CaZr_{1-x}Pu_xTi_2O_7$ system is reported to yield the zirconolite 3T polytype on reduction of Pu^{4+} to Pu^{3+} and zirconolite 3T natural analogues are generally characterised by a high fraction of trivalent lanthanides [49,50]. Hence, whilst $CaZrTi_2O_7$ can evidently be stabilised in the 3T polytype up to 1100 °C, incorporation of a significant Ce^{3+} may assist in stabilising this polytype to higher temperature as reported herein.

Perovskite is formed as an accessory phase in all products characterised in this study, with increased perovskite fraction correlated with increased Ce^{3+} fraction at constant synthesis temperature (1200 °C). As noted in the introduction, the formation of perovskite is undesirable since it has been shown to incorporate actinides but demonstrates comparably lower radiation tolerance and durability, with respect to zirconolite [51]. Nevertheless, the perovskite phase fraction could be reduced to 7.3 ± 1.0 wt.%, by adjusting the formulation to incorporate 10 wt.% ZrO_2 and 5 wt.% TiO_2, and sintering of the product powder, which is

comparable to the perovskite phase fraction in similar zirconolite compositions produced by reactive sintering in air [47].

5. CONCLUSION

Molten salt mediated synthesis of zirconolite ceramics, in the context of the decontamination of pyroprocessing molten salt wastes to yield a zirconolite ceramic, has some potential. However, this approach would not offer any clear benefit over oxygen sparging of the salt to precipitate lanthanides and minor actinides as oxides, followed by recovery and immobilisation in a glass or ceramic matrix, since both processes would require subsequent high temperature melting or reactive sintering steps to produce a wasteform monolith. Likewise, in the context of plutonium stockpile immobilisation, although molten salt mediated synthesis of zirconolite reduces the required reaction time and temperature, the subsequent requirement for a consolidation step means that the molten salt method does not offer a compelling advantage. Nevertheless, this work has served to usefully clarify mechanistic aspects of the molten salt mediated synthesis of zirconolite which should inform future application of molten salt technology in the nuclear and wider fields.

Acknowledgements

ARM is funded by the Engineering, Physical Sciences Research Council via the Next Generation Nuclear Centre for Doctoral Training (Grant EP/L015390/1). This research was supported in part by EPSRC under grant reference EP/S011935/1 and EP/R511754/1. NCH is grateful to the Royal Academy of Engineering and Nuclear Decommissioning Authority for funding. This research utilised the HADES/MIDAS facility at the University of Sheffield established with financial support from EPSRC and BEIS, under grant EP/T011424/1 [52]. With thanks to Dr C. Shaw at the Sorby Centre for Electron Microscopy, University of Sheffield for assistance with SEM imaging. This research used beamline 6-BM of the National Synchrotron Light Source II, a U.S. Department of Energy (DOE) Office of Science User Facility Operated for the DOE office of Science by Brookhaven National Laboratory under Contract No. DE-SC0012704; the authors are grateful to Dr B. Ravel, Dr D. Bailey and Ms. L. M. Mottram for experimental assistance.

References

[1] T. Nishimura, T. Koyama, M. Iizuka, H. Tanaka, Development of an environmentally benign reprocessing technology - pyrometallurgical reprocessing technology, Prog. Nucl. Energy. 32 (1998) 381–387. doi:10.1016/S0149-1970(97)00032-2.

[2] National Nuclear Laboratory, Advanced Reprocessing Research and Development Needs: Position Paper, Natl. Nucl. Lab. (2015). http://www.nnl.co.uk/media/1672/advanced-reprocessing-position-paper-final.pdf.

[3] I.W. Donald, Waste Immobilisation in Glass and Ceramic Based Hosts, Wiley, Chichester, 2010.

[4] A.R. Mason, S.M. Thornber, M.C. Stennett, L.J. Gardner, D. Lützenkirchen-Hecht, N.C. Hyatt, Preliminary investigation of chlorine speciation in zirconolite glass-ceramics for plutonium residues by analysis of Cl K-edge XANES, MRS Adv. (2019) 1–7. doi:10.1557/adv.2019.460.

[5] K.A. Evans, J.A. Mavrogenes, H.S. O'Neill, N.S. Keller, L.-Y.Y. Jang, A preliminary investigation of chlorine XANES in silicate glasses, Geochemistry, Geophys. Geosystems. 9 (2008). doi:10.1029/2008GC002157.

[6] D.A. McKeown, H. Gan, I.L. Pegg, W.C. Stolte, I.N. Demchenko, X-ray absorption studies of chlorine valence and local environments in borosilicate waste glasses, J. Nucl. Mater. 408 (2011) 236–245. doi:10.1016/j.jnucmat.2010.11.035.

[7] J.D. Webster, The exsolution of magmatic hydrosaline chloride liquids, Chem. Geol. 210 (2004) 33–48. doi:10.1016/j.chemgeo.2004.06.003.

[8] B.D. Begg, E.R. Vance, The incorporation of cerium in zirconolite, Mat. Res. Soc. Symp. Proc. 465 (1997) 333–340. doi:10.1557/PROC-465-333.

[9] M.R. Gilbert, C. Selfslag, M. Walter, M.C. Stennett, J. Somers, N.C. Hyatt, F.R. Livens, Synthesis and characterisation of Pu-doped zirconolites - $(Ca_{1-x}Pu_x)Zr(Ti_{2-2x}Fe_{2x})O_7$, IOP Conf. Ser. Mater. Sci. Eng. 9 (2010). doi:10.1088/1757-899X/9/1/012007.

[10] T.J. White, R.L.L. Segall, J.L.L. Hutchison, J.C.C. Barry, Polytypic behaviour of zirconolite, Proc. R. Soc. Lond. A. 392 (1984) 343–358. doi:10.1098/rspa.1984.0035.

[11] E.R. Vance, B.D. Begg, R.A. Day, C.J. Ball, Zirconolite rich ceramics for actinide wastes, Mat. Res. Soc. Symp. Proc. 353 (1995) 767–774.

[12] D. Caurant, P. Loiseau, I. Bardez, A. Quintas, Glasses, Glass-ceramics and Ceramics for Immobilization of Highly Radioactive Nuclear Wastes, Nova Science Publishers, 2009.

[13] G.R. Lumpkin, R.C. Ewing, B.C. Chakoumakos, R.B. Greegor, F.W. Lytle, E.M. Foltyn, F.W. Clinard, L.A. Boatner, M.M. Abraham, Alpha-recoil damage in zirconolite

($CaZrTi_2O_7$), J. Mater. Res. 1 (1986) 564–576. doi:10.1557/JMR.1986.0564.

[14] G.R. Lumpkin, R.C. Ewing, Geochemical alteration of pyrochlore group minerals: Betafite subgroup, Am. Mineral. 81 (1996) 1237–1248. doi:10.2138/am-1996-9-1022.

[15] G.R. Lumpkin, K.P. Hart, P.J. McGlinn, T.E. Payne, R. Gieré, C.T. Williams, Retention of actinides in natural pyrochlores and zirconolites, Radiochim. Acta. 66/67 (1994) 469–474. doi:10.1524/ract.1994.6667.s1.469.

[16] R. Gieré, C.T. Williams, G. Lumpkin, Chemical characteristics of natural zirconolite, Swiss Soc. Mineral. Petrol. 78 (1998) 433–459. doi:10.5169/seals-59299.

[17] M.L. Hand, M.C. Stennett, N.C. Hyatt, Rapid low temperature synthesis of a titanate pyrochlore by molten salt mediated reaction, J. Eur. Ceram. Soc. 32 (2012) 3211–3219. doi:10.1016/j.jeurceramsoc.2012.04.046.

[18] T. Advocat, F. Jorion, T. Marcillat, G. Leturcq, X. Deschanels, J.M. Boubals, L. Bojat, P. Nivet, S. Peuget, Fabrication of Pu-Zirconolite Ceramic Pellets by Natural Sintering, Mat. Res. Soc. Symp. Proc. 807 (2004) 1–5. doi:10.1557/PROC-807-267.

[19] M.R. Gilbert, Molten salt synthesis of zirconolite polytypes, Mat. Res. Soc. Symp. Proc. 1665 (2014) 325–330. doi:10.1557/opl.2014.662.

[20] T. Kimura, Molten Salt Synthesis of Ceramic Powders, in: C. Sikalidis (Ed.), Adv. Ceram. - Synth. Charact. Process. Specif. Appl., InTech Open, 2011: pp. 75–100. doi:10.5772/20472.

[21] Z. Li, W.E. Lee, S. Zhang, Low-Temperature Synthesis of $CaZrO_3$ Powder from Molten Salts, J. Am. Ceram. Soc. 90 (2007) 364–368. doi:10.1111/j.1551-2916.2006.01383.x.

[22] S. Zhang, Low Temperature Synthesis of Complex Refractory Oxide Powders From Molten Salts, J. Pakistan Mater. Soc. 1 (2007) 49–53.

[23] S. Zhang, D.D. Jayaseelan, G. Bhattacharya, W.E. Lee, Molten salt synthesis of magnesium aluminate ($MgAl_2O_4$) spinel powder, J. Am. Ceram. Soc. 89 (2006) 1724–1726. doi:10.1111/j.1551-2916.2006.00932.x.

[24] S. Hashimoto, S. Zhang, W.E. Lee, A. Yamaguchi, Synthesis of Magnesium Aluminate Spinel Platelets from α-Alumina Platelet and Magnesium Sulfate Precursors, J. Am. Ceram. Soc. 86 (2003) 1959–1961. doi:10.1111/j.1151-2916.2003.tb03589.x.

[25] X. Liu, S. Zhang, Low-temperature preparation of titanium carbide coatings on graphite flakes from molten salts, J. Am. Ceram. Soc. 91 (2008) 667–670. doi:10.1111/j.1551-2916.2007.02184.x.

[26] S.M. Thornber, P.G. Heath, G.P. Da, M.C. Stennett, N.C. Hyatt, The effect of pre-treatment parameters on the quality of glass-ceramic wasteforms for plutonium immobilisation, consolidated by hot isostatic pressing, J. Nucl. Mater. 485 (2017). doi:10.1016/j.jnucmat.2016.12.028.

[27] N.C. Hyatt, Plutonium management policy in the United Kingdom: The need for a dual track strategy, Energy Policy. 99 (2016). doi:10.1016/j.enpol.2016.08.033.

[28] K. Webb, R. Taylor, C. Campbell, M. Carrott, C. Gregson, J. Hobbs, F. Livens, C. Maher, R. Orr, H. Sims, H. Steele, S. Sutherland-Harper, Thermal Processing of Chloride-Contaminated Plutonium Dioxide, ACS Omega. 4 (2019) 12524–12536. doi:10.1021/acsomega.9b00719.

[29] S. Sutherland-Harper, F. Livens, C. Pearce, J. Hobbs, R. Orr, R. Taylor, K. Webb, N. Kaltsoyannis, Interactions of HCl and H_2O with the surface of PuO_2, J. Nucl. Mater. 518 (2019) 256–264. doi:10.1016/j.jnucmat.2019.02.036.

[30] M.R. Gilbert, J.H. Harding, Energetics of Ce and Pu incorporation into zirconolite waste-forms., Phys. Chem. Chem. Phys. 13 (2011) 13021–13025. doi:10.1039/c0cp01478h.

[31] C. Lopez, X. Deschanels, J.M. Bart, J.M. Boubals, C. Den Auwer, E. Simoni, Solubility of actinide surrogates in nuclear glasses, J. Nucl. Mater. 312 (2003) 76–80. doi:10.1016/S0022-3115(02)01549-0.

[32] P.A. Bingham, R.J. Hand, M.C. Stennett, N.C. Hyatt, M.T. Harrison, The Use of Surrogates in Waste Immobilization Studies: A Case Study of Plutonium, Mater. Res.

Soc. Symp. Proc. 1107 (2008). doi:10.1557/PROC-1107-421.

[33] National Reserch Council, Electrometallurgical Techniques for DOE Spent Fuel Treatment, National Academy Press, Washington DC, 2000. doi:10.17226/9883.

[34] Department of Energy and Climate Change, Management of the UK's Plutonium Stocks: A consultation response on the proposed justification process for the reuse of plutonium, 2013.

[35] OECD Nuclear Energy Agency, Pyrochemical Separations in Nuclear Applications, A Status Report, 2004. http://www.oecd.org/.

[36] A.A. Coelho, J. Evans, I. Evans, A. Kern, S. Parsons, The TOPAS symbolic computation system, Powder Diffr. 26 (2011) 22–25. doi:10.1154/1.3661087.

[37] J.C. Woicik, B. Ravel, D.A. Fischer, W.J. Newburgh, Performance of a four-element Si drift detector for X-ray absorption fine-structure spectroscopy: Resolution, maximum count rate, and dead-time correction with incorporation into the ATHENA data analysis software, J. Synchrotron Radiat. 17 (2010) 409–413. doi:10.1107/S0909049510009064.

[38] J.A. Bearden, A.F. Burr, Reevaluation of X-ray atomic energy levels, Rev. Mod. Phys. 39 (1967) 125–142. doi:10.1103/RevModPhys.39.125.

[39] B. Ravel, M. Newville, ATHENA, ARTEMIS, HEPHAESTUS: Data analysis for X-ray absorption spectroscopy using IFEFFIT, J. Synchrotron Radiat. 12 (2005) 537–541. doi:10.1107/S0909049505012719.

[40] B.D. Begg, E.R. Vance, G.R. Lumpkin, Charge Compensation and the Incorporation of Cerium in Zirconolite and Perovskite, Mat. Res. Soc. Symp. Proc. 506 (1998) 79–86. doi:10.1557/proc-506-79.

[41] Y.Z. Cho, G.H. Park, H.C. Yang, D.S. Han, H.S. Lee, I.T. Kim, Minimization of eutectic salt waste from pyroprocessing by oxidative precipitation of lanthanides, J. Nucl. Sci. Technol. 46 (2009) 1004–1011. doi:10.1080/18811248.2009.9711610.

[42] D.P. Reid, M.C. Stennett, N.C. Hyatt, The fluorite related modulated structures of the

$Gd_2(Zr_{2-x}Ce_x)O_7$ solid solution: An analogue for Pu disposition, J. Solid State Chem. 191 (2012) 2–9. doi:10.1016/j.jssc.2011.12.039.

[43] M.C. Stennett, C.L. Freeman, A.S. Gandy, N.C. Hyatt, Crystal structure and non-stoichiometry of cerium brannerite: $Ce_{0.975}Ti_2O_{5.95}$, J. Solid State Chem. 192 (2012) 172–178. doi:10.1016/j.jssc.2012.03.057.

[44] A. V. Soldatov, T.S. Ivanchenko, S. Della Longa, A. Kotani, Y. Iwamoto, A. Bianconi, Crystal-structure effects in the Ce L_3-edge X-ray-absorption spectrum of CeO_2: Multiple-scattering resonances and many-body final states, Phys. Rev. B. 50 (1994) 5074–5080. doi:10.1103/PhysRevB.50.5074.

[45] A. Bianconi, A. Marcelli, H. Dexpert, R. Karnatak, A. Kotani, T. Jo, J. Petiau, Specific intermediate-valence state of insulating 4f compounds detected by L_3 X-ray absorption, Phys. Rev. B. 35 (1987) 806–812. doi:10.1103/PhysRevB.35.806.

[46] C.L. Corkhill, D.J. Bailey, F.Y. Tocino, M.C. Stennett, J.A. Miller, J.L. Provis, K.P. Travis, N.C. Hyatt, Role of Microstructure and Surface Defects on the Dissolution Kinetics of CeO_2, a UO_2 Fuel Analogue, ACS Appl. Mater. Interfaces. 8 (2016) 10562–10571. doi:10.1021/acsami.5b11323.

[47] L.R. Blackburn, S. Sun, L.J. Gardner, E.R. Maddrell, C. Martin, N.C. Hyatt, A systematic investigation of the phase assemblage and microstructure of the zirconolite $CaZr_{1-x}Ce_xTi_2O_7$ system, J. Nucl. Mater. (2020). doi:10.1016/j.jnucmat.2020.152137.

[48] Y.P. Lan, H.Y. Sohn, A. Murali, J. Li, C. Chen, The formation and growth of CeOCl crystals in a molten KCl-LiCl flux, Appl. Phys. A Mater. Sci. Process. 124 (2018) 1–6. doi:10.1007/s00339-018-2122-3.

[49] B.D. Begg, R.A. Day, A. Brownscombe, Structural effect of Pu substitutions on the Zr-site in zirconolite, Mat. Res. Soc. Symp. Proc. 663 (2001). doi:10.1557/PROC-663-259.

[50] N. V. Zubkova, N. V. Chukanov, I. V. Pekov, B. Ternes, W. Schüller, D.A. Ksenofontov, D.Y. Pushcharovsky, The crystal structure of nonmetamict Nb-rich zirconolite-3T from

the Eifel paleovolcanic region, Germany, Zeitschrift Fur Krist. - Cryst. Mater. 233 (2018) 463–468. doi:10.1515/zkri-2017-2133.

[51] K.L. Smith, G.R. Lumpkin, M.G. Blackford, R.A. Day, K.P. Hart, The durability of synroc, J. Nucl. Mater. 190 (1992) 287–294. doi:10.1016/0022-3115(92)90092-Y.

[52] N.C. Hyatt, C.L. Corkhill, M.C. Stennett, R.J. Hand, L.J. Gardner, C.L. Thorpe, The HADES Facility for High Activity Decommissioning Engineering & Science : part of the UK National Nuclear User Facility, IOP Conf. Ser. Mater. Sci. Eng. 818 (2020) 1–8. doi:10.1088/1757-899X/818/1/012022.

Figure Captions

Fig. 1. XRD patterns of $Ca_{0.9}Zr_{0.9}Ce_{0.2}Ti_2O_7$ MSS with synthesis temperature: (i) 1400 °C (ii) 1300 °C (iii) 1200 °C (iv) 1100 °C; the reaction time was 2h in air. Miller indices highlight major reflections of the zirconolite 2M phase. Primary diagnostic reflections of reagents and accessory phases are indicated by: P, $CaTiO_3$ perovskite; T, TiO_2 rutile; Z, ZrO_2; C, CeO_2.

Fig. 2. Quantitative phase analysis of XRD data of MSS products shown in Fig. 1 and Fig. 3-5; “excess” denotes addition of 10 wt.% ZrO_2 and 5 wt.% TiO_2 to stoichiometric formulation. Unless otherwise stated MSS was performed at 1200 °C for 2 h in air with CeO_2 as the Ce source.

Fig. 3. XRD patterns of $Ca_{0.9}Zr_{0.9}Ce_{0.2}Ti_2O_7$ MSS at 1200 °C for 2 h, with synthesis atmospheres: (i) air (ii) 5% H_2/N_2 (iii) Ar. Miller indices highlight major reflections of the zirconolite 2M phase. Primary diagnostic reflections of reagents and accessory phases are indicated by: P, $CaTiO_3$ perovskite; T, TiO_2; Z, ZrO_2; C, CeO_2.

Fig. 4. XRD patterns of $Ca_{0.9}Zr_{0.9}Ce_{0.2}Ti_2O_7$ MSS at 1200 °C in air with furnace dwell durations: (i) 8 h (ii) 4 h (iii) 2 h. Miller indices highlight major reflections of the zirconolite 2M phase. Primary diagnostic reflections of reagents and accessory phases are indicated by: P, $CaTiO_3$ perovskite; T, TiO_2; Z, ZrO_2; C, CeO_2.

Fig. 5. XRD patterns of $Ca_{0.9}Zr_{0.9}Ce_{0.2}Ti_2O_7$ MSS with additional excesses of 10 wt.% ZrO_2 and 5 wt.% TiO_2, and $CeCl_3$ reagent where indicated: (i) 1200 °C, $CeCl_3$, 10 wt.% ZrO_2 and 5 wt.% TiO_2 (ii) 1200 °C, $CeCl_3$ (iii) 1200 °C,10 wt.%

678 ZrO_2 and 5 wt.% TiO_2 (iv) 1200 °C; the reaction time was 2 h, in air. Miller
679 indices highlight major reflections of the zirconolite 2M phase. Primary
680 diagnostic reflections of reagents and accessory phases are indicated by: P,
681 $CaTiO_3$ perovskite; T, TiO_2; Z, ZrO_2; C, CeO_2.

682 Fig. 6. XRD patterns to compare; (i) the product of a secondary sintering
683 process (1350 °C, for 20 h, in air) of the MSS product in (ii), (ii)
684 $Ca_{0.9}Zr_{0.9}Ce_{0.2}Ti_2O_7$ MSS; 1200 °C for 2 h in air. Miller indices highlight major
685 reflections of the zirconolite 2M phase. Primary diagnostic reflections of
686 reagents and accessory phases are indicated by: P, $CaTiO_3$ perovskite; T, TiO_2;
687 Z, ZrO_2; C, CeO_2.

688 Fig. 7. SEM micrographs, in secondary electron mode, of: (A) TiO_2 (B) CeO_2 (C)
689 ZrO_2 (D) $Ca_{0.9}Zr_{0.9}Ce_{0.2}Ti_2O_7$ from MSS at 1200 °C, for 2h, in air.

690 Fig. 8. SEM micrograph, in SE mode, of the surface of the ceramic produced
691 after sintering of MSS product at 1350 °C for 20 h, in air, highlighting
692 component phases: accessory phases are indicated by: P, perovskite; Z, ZrO_2;
693 and zirconolite 2M and 4M polymorphs. Representative EDX spectrum of the
694 zirconolite 2M phase is shown.

695 Fig. 9. Ce L_3 XANES spectra of recovered product of $Ca_{0.9}Zr_{0.9}Ce_{0.2}Ti_2O_7$ MSS
696 in air, compared with $CePO_4$, $CeAlO_3$ and CeO_2 reference compounds: A)
697 reaction at 1100 – 1400 °C for 2 h, in air; B) reaction at 1200 °C for 2 h using
698 flowing 5% H_2/N_2, Ar or air; C) reaction at 1200 °C for 2 – 8 h, in air; D) reaction
699 at 1200 °C for 2 h, in air, using CeO_2 or $CeCl_3.7H_2O$ as Ce source, with / without
700 10 wt.% ZrO_2 and 5 wt.% TiO_2 excess.

Fig. 10. Comparison of quantity of Ce^{3+} and perovskite weight fraction in product materials. Black squares represent all MSS zirconolite materials produced at 1200 °C. Blue circles represent MSS zirconolite materials produced at temperatures other than 1100 °C, 1300 °C and 1400 °C.

705 **Tables**

Temperature (°C)	Time (h)	Atmosphere	Reagent	Excess	Phase fraction (wt.%)						
					$CaTiO_3$ (± 1.0)	CeO_2 (± 0.07)	TiO_2 (± 0.2)	Z-2M (± 1.8)	Z-3T (± 1.5)	Z-4M (± 1.5)	ZrO_2 (± 0.4)
1100	2	air	CeO_2	-	32.8	0.40	2.1	43.9	11.0	0	9.7
1200	2	air	CeO_2	-	28.1	0.16	1.7	52.2	14.7	0	3.0
1300	2	air	CeO_2	-	27.3	0.20	2.1	52.4	15.8	0	2.1
1400	2	air	CeO_2	-	24.8	0.27	0.2	62.1	12.2	0	0.3
1200	4	air	CeO_2	-	27.5	1.11	1.7	56.7	9.8	0	3.9
1200	8	air	CeO_2	-	26.6	0.62	0.2	53.8	16.2	0	2.4
1200	2	air	CeO_2	✓	9.4	0.26	1.8	64.3	19.3	0	3.9
1200	2	air	$CeCl_3$	-	25.4	0.62	3.0	47.1	15.7	0	8.0
1200	2	air	$CeCl_3$	✓	15.4	0.33	3.7	48.5	20.4	0	11.5
1200	2	5% H_2/N_2	CeO_2	-	33.3	0.58	2.1	30.7	15.9	0	17.2
1200	2	Ar	CeO_2	-	40.9	0.28	8.4	29.1	5.7	0	15.6
1350**	20	air	CeO_2	-	7.3	0.12	0.1	75.9	5.8	10.0	0.7

706

707 Table 1. Quantitative analysis using Rietveld refinement on XRD patterns in Fig. 1 and Fig. 3-5; “excess” denotes addition of
708 10 wt.% ZrO_2 and 5 wt.% TiO_2 to stoichiometric formulation. ** Refers to the material produced after the secondary sintering of
709 the MSS material formed at 1200 °C for 2 h in air with CeO_2 as the surrogate.

Temperature (°C)	Time (h)	Atmosphere	Reagent	Excess	Ce^{3+} (%)
1100	2	Air	CeO_2	-	54 ± 3
1200	2	Air	CeO_2	-	59 ± 3
1300	2	Air	CeO_2	-	62 ± 3
1400	2	Air	CeO_2	-	71 ± 3
1200	4	Air	CeO_2	-	62 ± 3
1200	8	Air	CeO_2	-	53 ± 3
1200	2	Air	CeO_2	✓	33 ± 3
1200	2	Air	$CeCl_3$	-	38 ± 3
1200	2	Air	$CeCl_3$	✓	33 ± 3
1200	2	5% H_2/N_2	CeO_2	-	100 ± 4
1200	2	Ar	CeO_2	-	100 ± 4

710

711 Table 2. Results of linear combination fitting of spectra from Fig. 9.; “excess” denotes addition of 10 wt.% ZrO_2 and 5 wt.%

712 TiO_2 to the stoichiometric formulation.

713

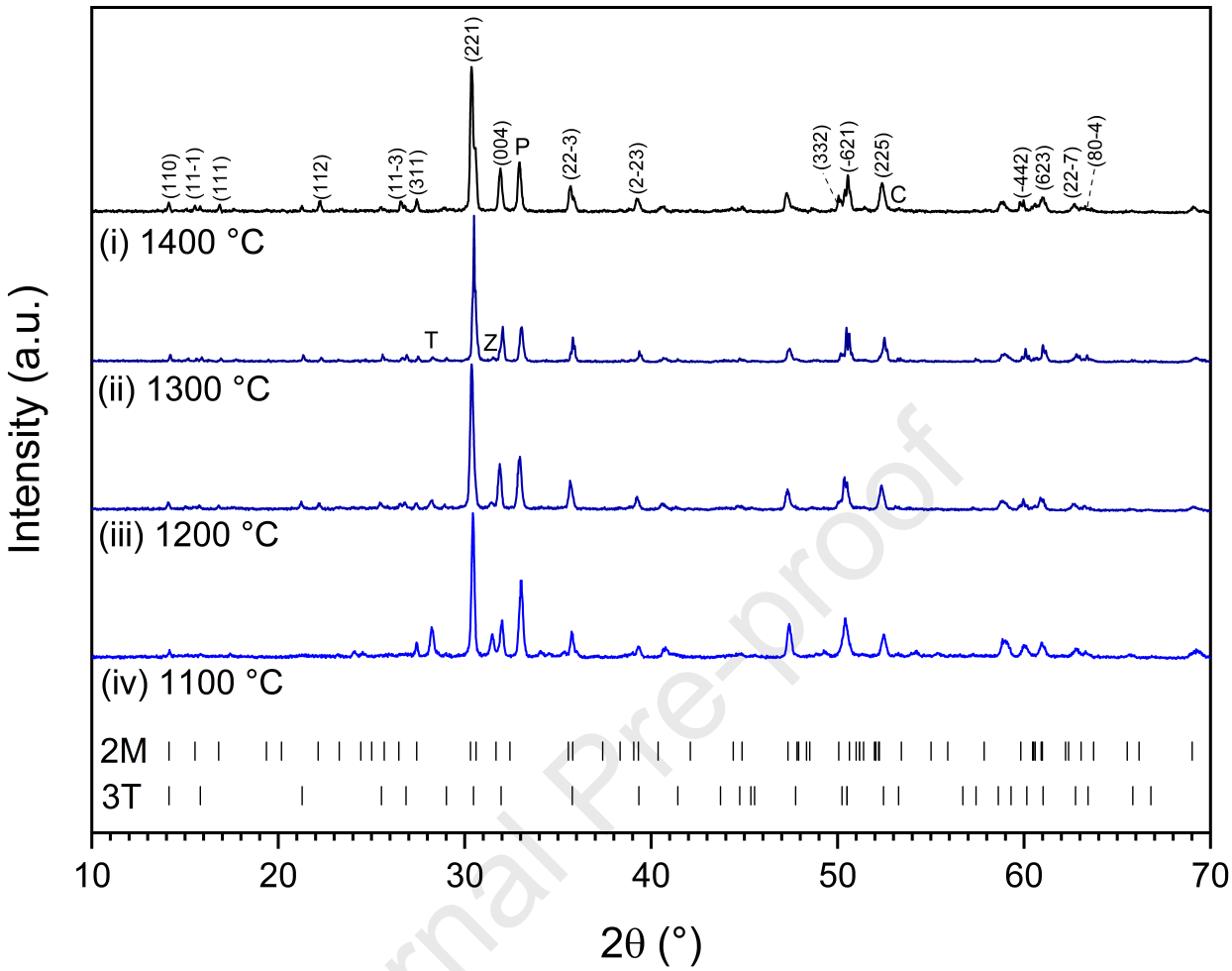

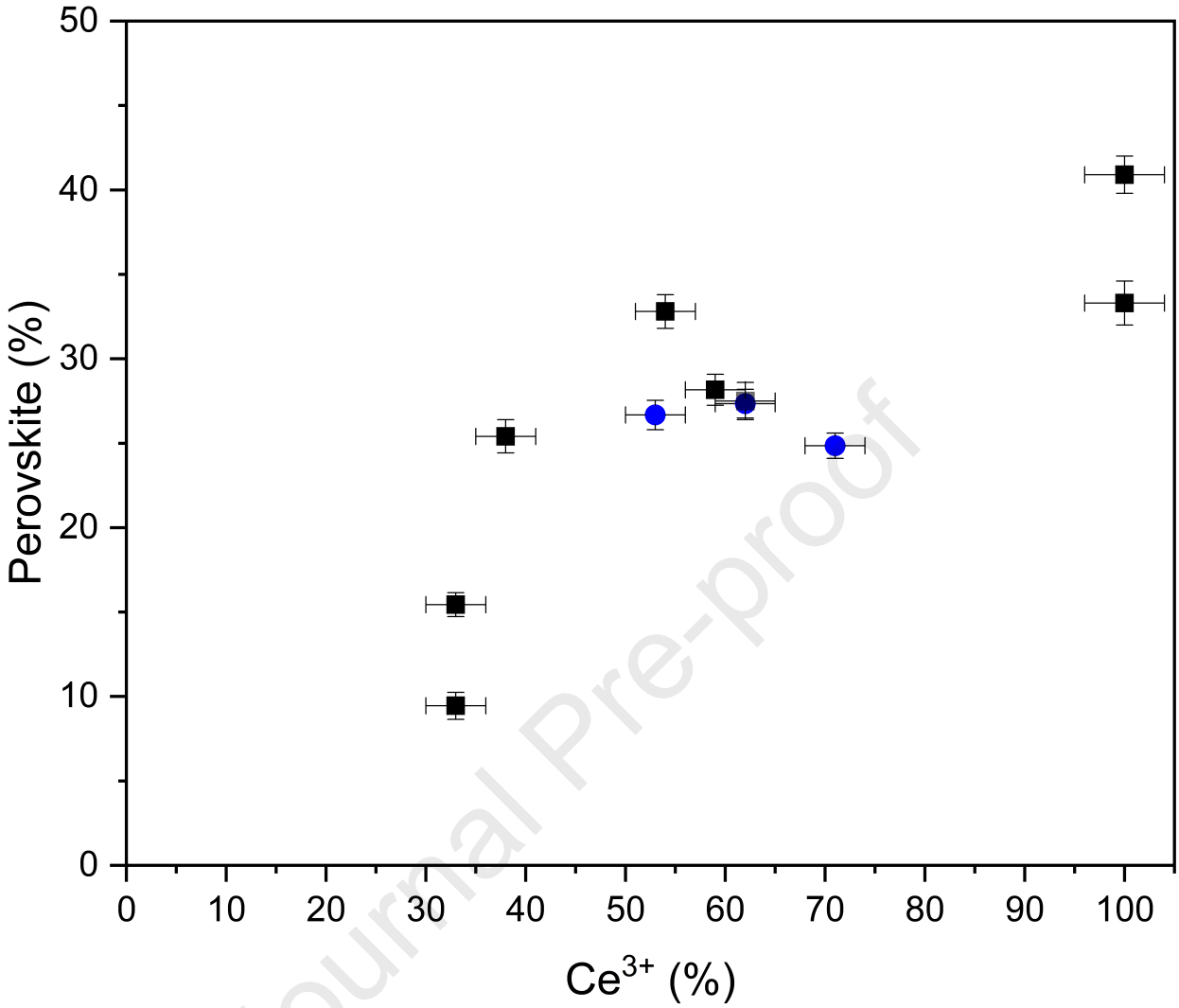

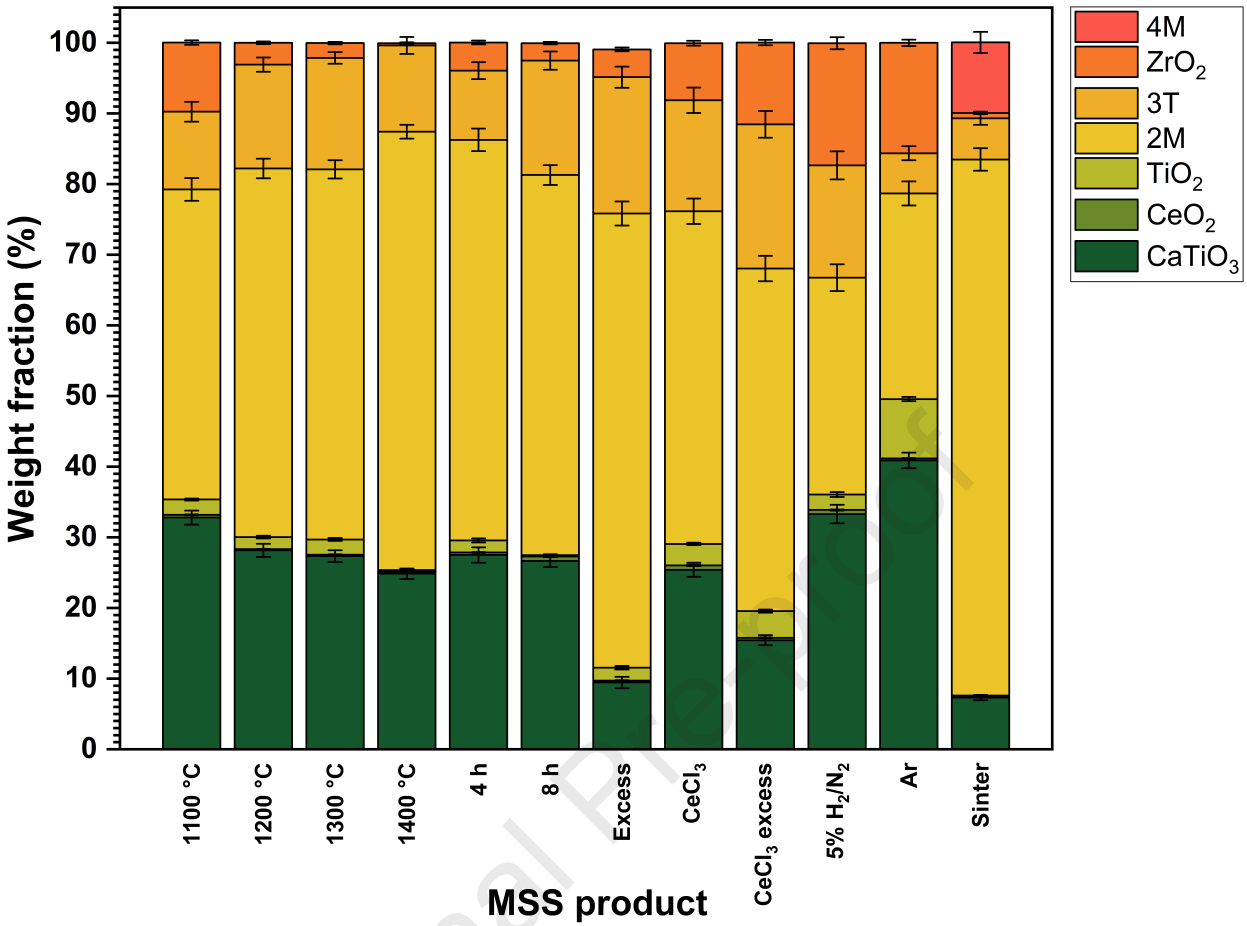

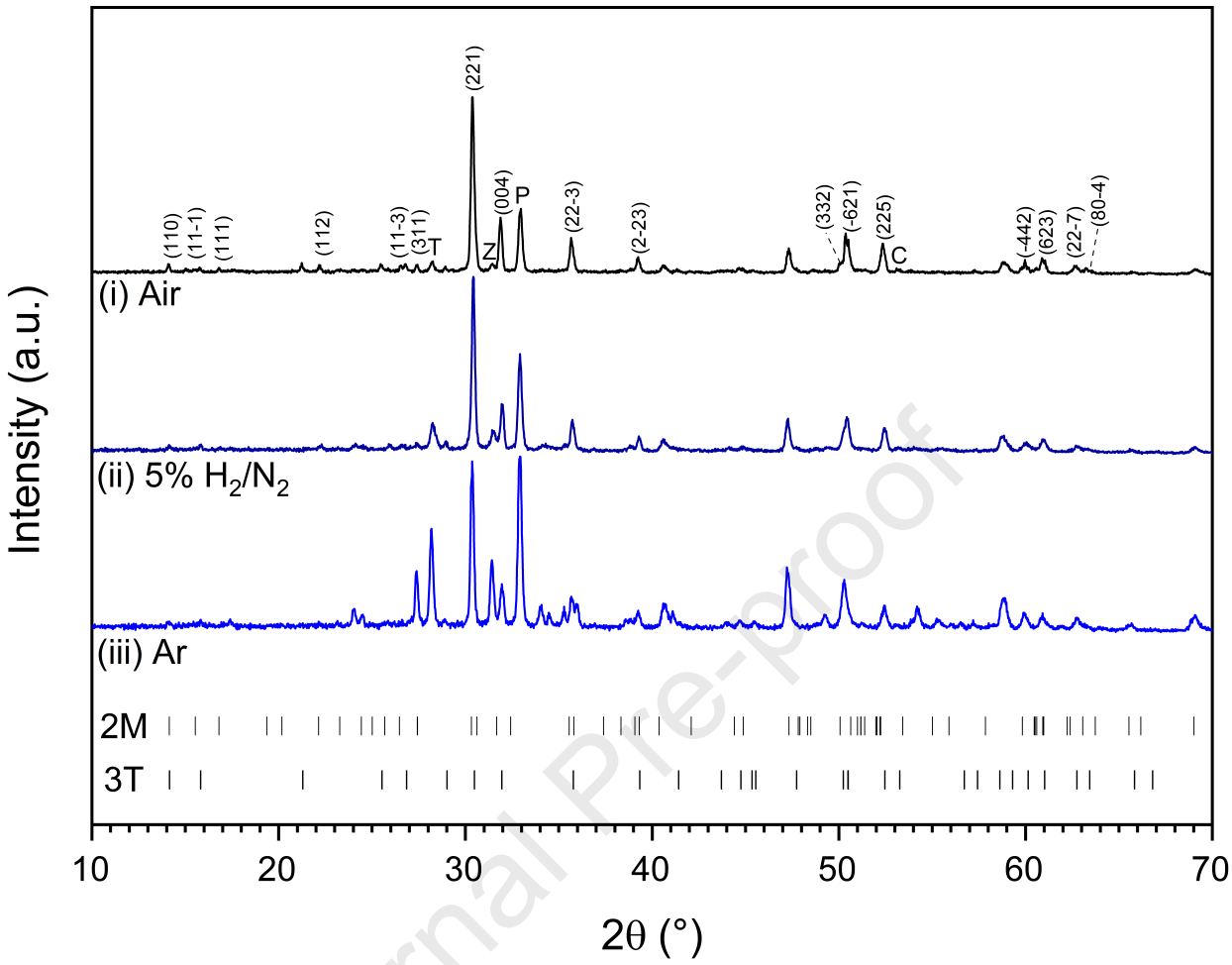

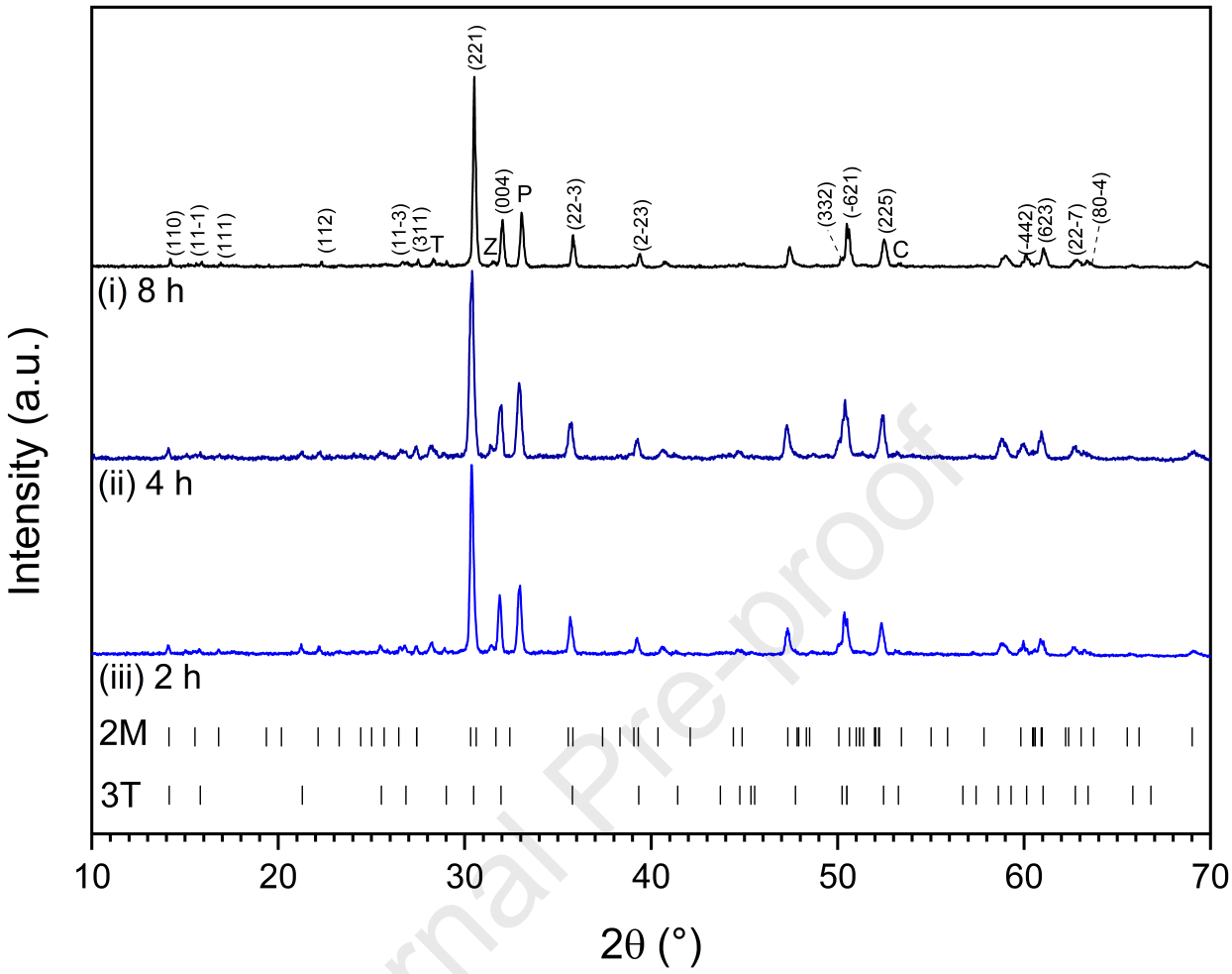

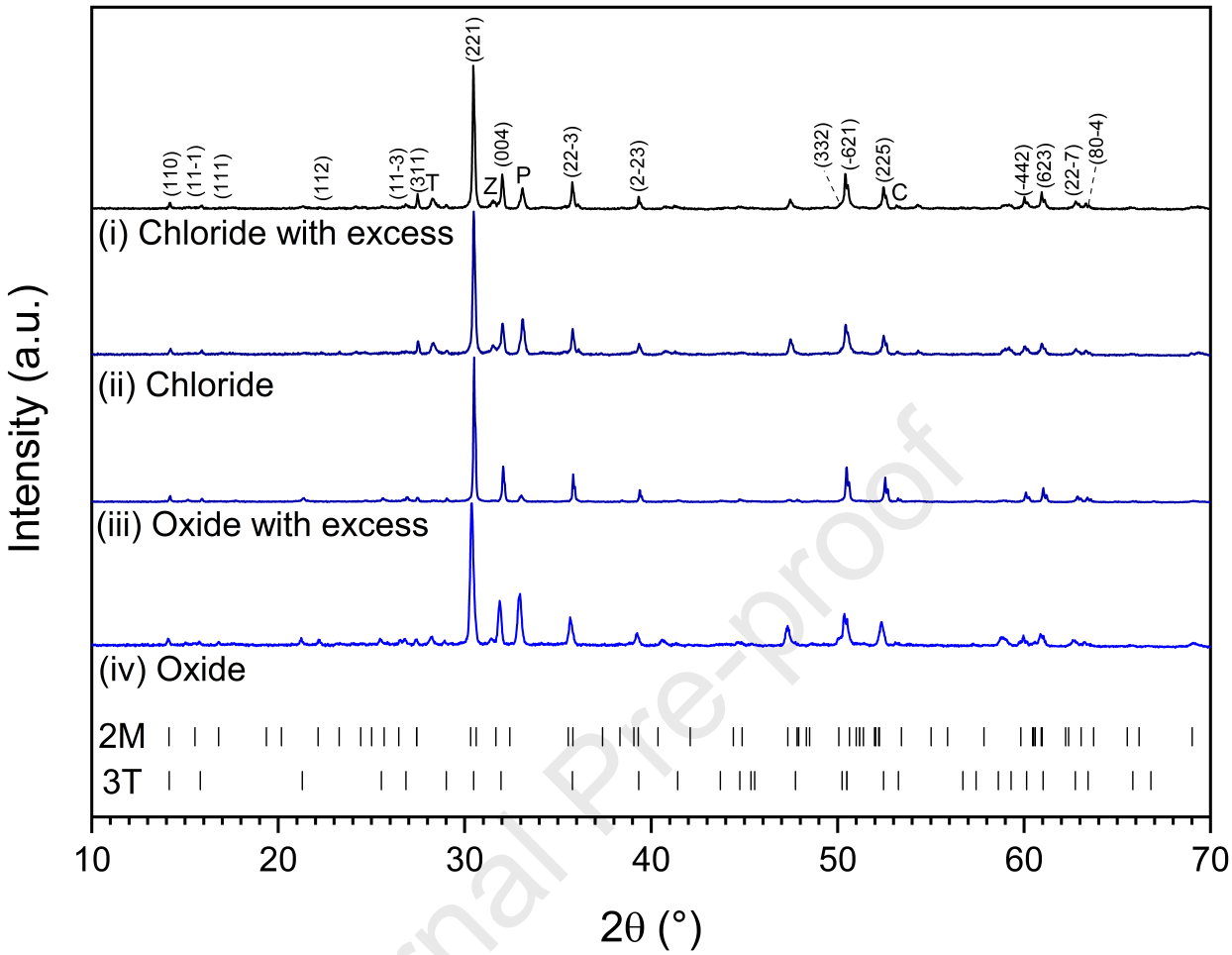

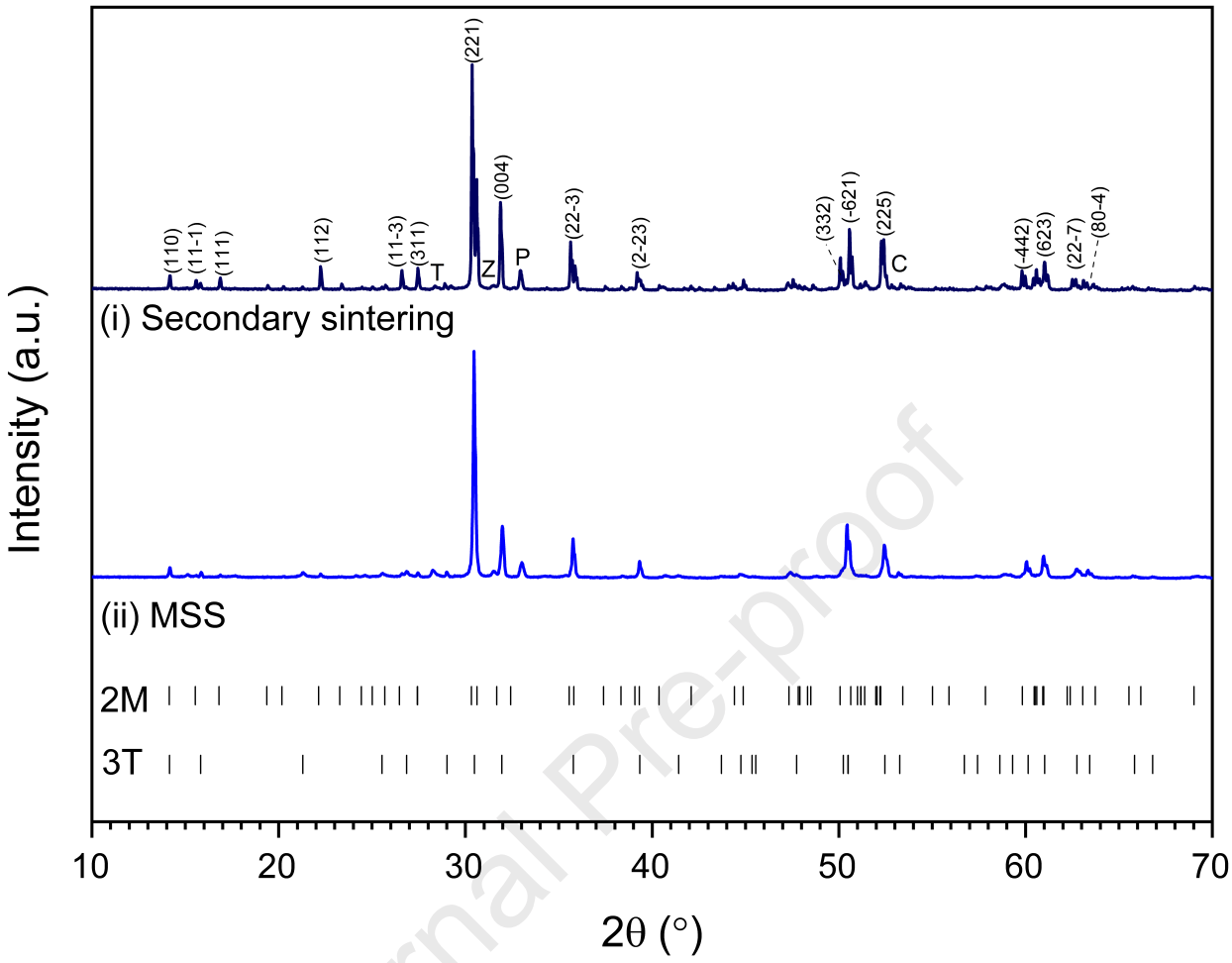

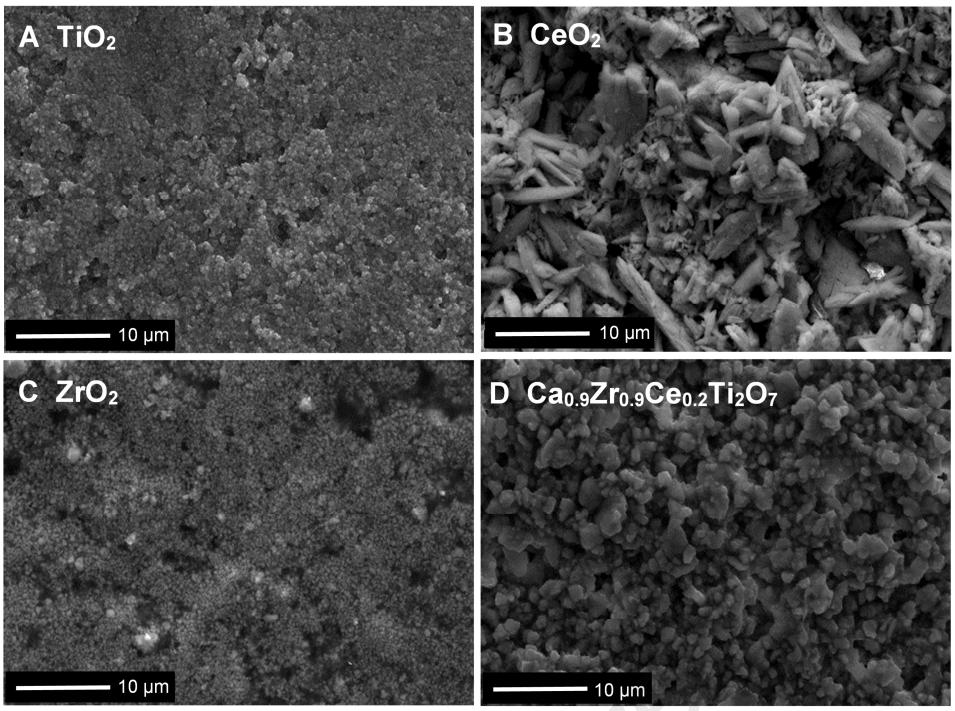

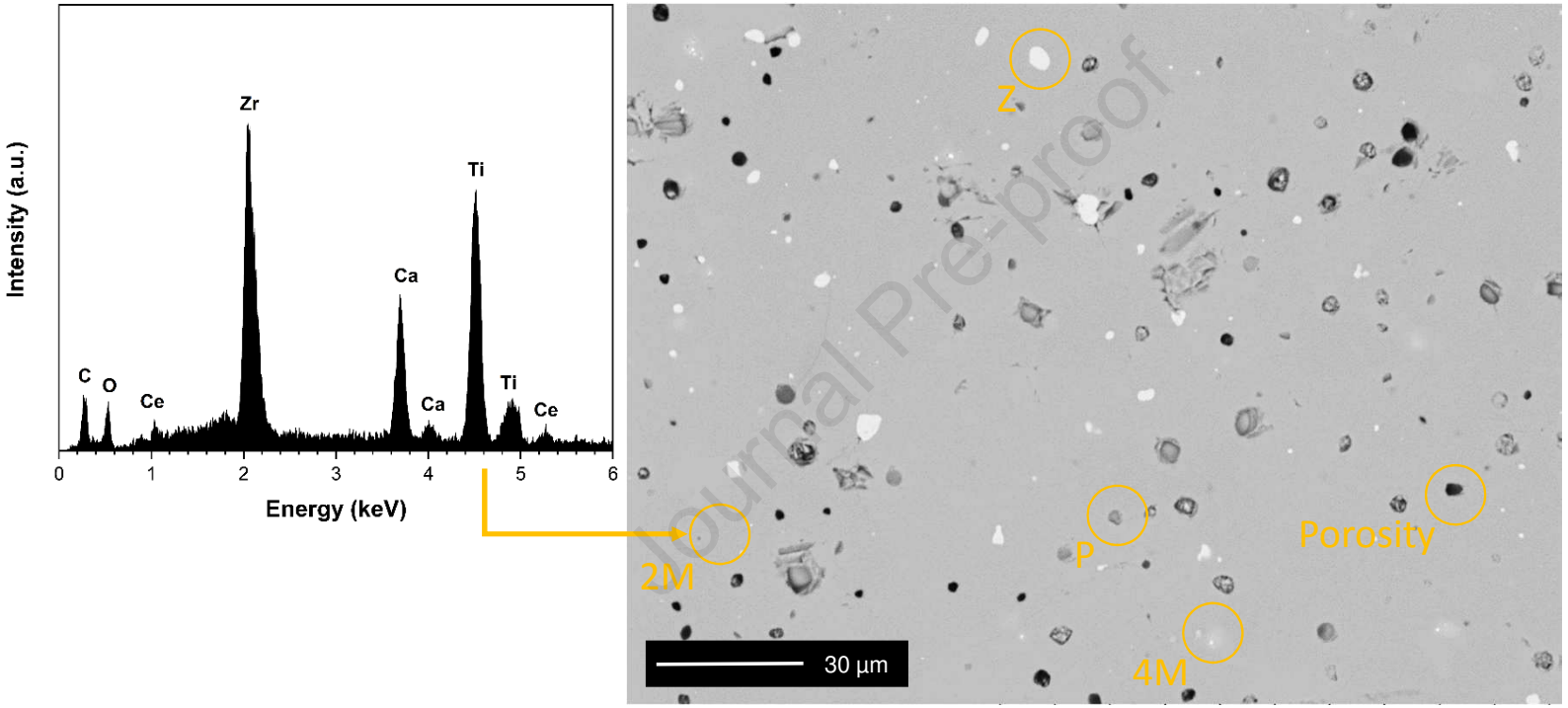

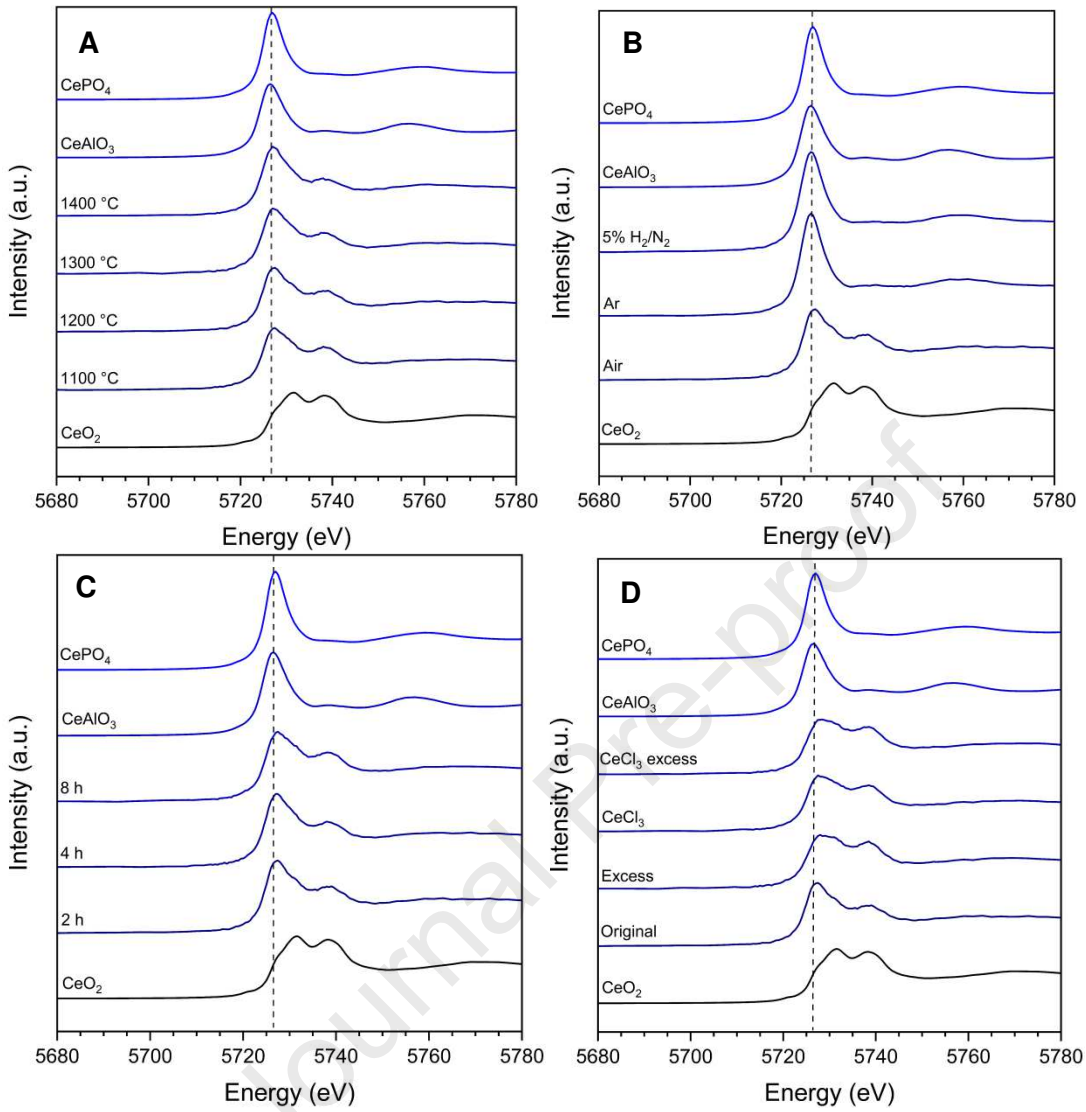

The University Of Sheffield.

Department Of Materials Science and Engineering

Professor Neil Hyatt
Royal Academy of Engineering Chair in Radioactive Waste Management
Professor of Nuclear Materials Chemistry
Sir Robert Hadfield Building
Mappin Street
Sheffield S1 3JD
United Kingdom
Telephone: +44 (0) 114 222 5502
e-mail: n.c.hyatt@sheffield.ac.uk

30 July 2020

Dear Editor,

I am pleased to submit the attached revised manuscript titled *"Molten salt synthesis of Ce doped zirconolite for the immobilisation of pyroprocessing wastes and separated plutonium"* by Mason *et al.*, to be considered for publication in Ceramics International. I confirm that the manuscript is not under consideration for publication elsewhere, that its publication is approved by all authors, and that, if accepted, it will not be published elsewhere in the same form, in English or in any other language, including electronically without the written consent of the copyright-holder.

The manuscript has been amended in response to each comment from the two reviewers, with the requested change being implemented in each case. This is detailed in the attached "Response to Reviewers" documents. We have also made some minor changes to the text and tables to improve clarity, prompted by feedback from the reviewers, including the addition of three supplementary figures for completeness.

On behalf of the co-authors may I take this opportunity to thank the two reviewers for their careful reading of the manuscript and suggestions for improvement, and also the editorial team for their handling of the manuscript at this challenging time.

Thank you for your consideration of our manuscript. Please contact me at the above email address with correspondence.

Yours sincerely

Neil Hyatt

Professor Neil Hyatt.

Declaration of interests

☒ The authors declare that they have no known competing financial interests or personal relationships that could have appeared to influence the work reported in this paper.

☐The authors declare the following financial interests/personal relationships which may be considered as potential competing interests: